molecular pharmaceutics

Article

Cite This: *Mol. Pharmaceutics* 2019, 16, 3711−3719

pubs.acs.org/molecularpharmaceutics

Oncoprotein Inhibitor Rigosertib Loaded in ApoE-Targeted Smart Polymersomes Reveals High Safety and Potency against Human Glioblastoma in Mice

Huazhen Qin, Yu Jiang, Jian Zhang, Chao Deng,* and Zhiyuan Zhong*

Biomedical Polymers Laboratory, and Jiangsu Key Laboratory of Advanced Functional Polymer Design and Application, College of Chemistry, Chemical Engineering and Materials Science, and State Key Laboratory of Radiation Medicine and Protection, Soochow University, Suzhou 215123, China

Supporting Information

ABSTRACT: The unbiased cytotoxicity and blood−brain barrier (BBB) impermeability render common chemotherapeutics nonviable for treating glioblastoma (GBM) patients. Although rigosertib (RGS), a RAS effector protein inhibitor, has shown low toxicity to healthy cells and high efficacy toward various cancer cells by inactivating PI3K-Akt, it hardly overcomes the BBB barricade. Here, we report that RGS loaded in apolipoprotein E derived peptide (ApoE)-targeted chimaeric polymersomes (ApoE-CP) is safe and highly potent against human GBM in vivo. ApoE-CP exhibited stable loading of RGS in its lumen, giving RGS nanoformulations (ApoE-CP-RGS) with a size of 60 nm and reduction-triggered drug release behavior. Notably, ApoE-CP-RGS induction markedly enhanced the G2/M cell cycle arrest and inhibitory effect in U-87 MG glioblastoma cells compared with the nontargeted CP-RGS and free RGS. The therapeutic outcomes in orthotopic U-87 MG GBM models demonstrated that ApoE-CP-RGS brought about effective GBM inhibition, greatly prolonged survival time, and depleted adverse effects. Rigosertib formulated in ApoE-targeted chimaeric polymersomes has emerged as a novel, highly specific, efficacious, and nontoxic treatment for glioblastoma.

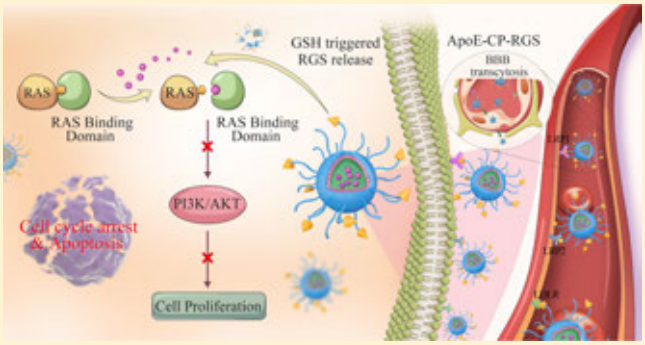

KEYWORDS: *brain tumor, RAS inhibitor, nanomedicines, blood−brain barrier, targeted delivery*

INTRODUCTION

Glioblastoma (GBM) remains a formidable malignancy. The expected survival time for GBM patients receiving state-of-the-art regimen (including surgical resection, radiotherapy, and/or temozolomide chemotherapy) is only 15 months.[1,2] The common chemotherapeutics have typically low blood−brain barrier (BBB) permeability, rendering them invalid for treatment of GBM.[3−5] Interestingly, nanomedicines functionalized with several ligands such as transferrin,[6−10] apolipoprotein,[11−13] glucose,[14,15] and angiopep-2 peptides[16−21] are found to be BBB permeable and can largely enhance the drug concentration in GBM. Angiopep-2 peptides/paclitaxel conjugate has been used to treat brain metastases in phase I clinical trial.[22] These BBB-permeable nanomedicines, though showing enhanced inhibition of GBM, have not negated the side effects associated with the unbiased cytotoxicity of drug payloads.

The activation of oncogenic RAS subfamily of genes, including HRAS, KRAS, and NRAS, is closely associated with the occurrence of human cancers.[23,24] The main three RAS effector proteins are RAF, RalGDS, and phosphoinositide-3 kinases (PI3K), which share a common RAS-binding domain (RBD) and mediate the activation of the PI3K pathway.[25,26] Rigosertib (RGS, also known as Estybon or ON 01910) is a RAS-mimetic small-molecule inhibitor of the interactions of RAS and effector proteins by binding to RBDs.[27,28] The inhibition of effector proteins will result in the inactivation of RAF, RalGDS, and PI3K-Akt pathway, and finally lead to the G2/M cell cycle arrest and apoptosis of cancer cells.[29−31] RGS showed significant growth inhibition against a host of human cancer cells but low toxicity to healthy cells,[29,30,32] and is currently under extensive clinical investigations for indications of myelodysplastic syndrome (phase III, NCT01241500),[33] squamous cell carcinoma (phase II, NCT01807546),[34] acute myelocytic leukemia (phase I/II, NCT01167166),[35] and metastatic pancreatic cancer (phase III, NCT01360853).[36] However, as for most chemical drugs, RGS has low BBB permeability. GBM is an "undrugable" target[37] for RGS.

Received: June 25, 2019
Revised: June 28, 2019
Accepted: July 1, 2019
Published: July 12, 2019

DOI: 10.1021/acs.molpharmaceut.9b00691
Mol. Pharmaceutics 2019, 16, 3711−3719

Scheme 1. Rigosertib (RGS)-Loaded ApoE-Targeted Smart Polymersomes (ApoE-CP-RGS) for Safe and Highly Potent Treatment of Human Glioblastoma (GBM) in Mice[a]

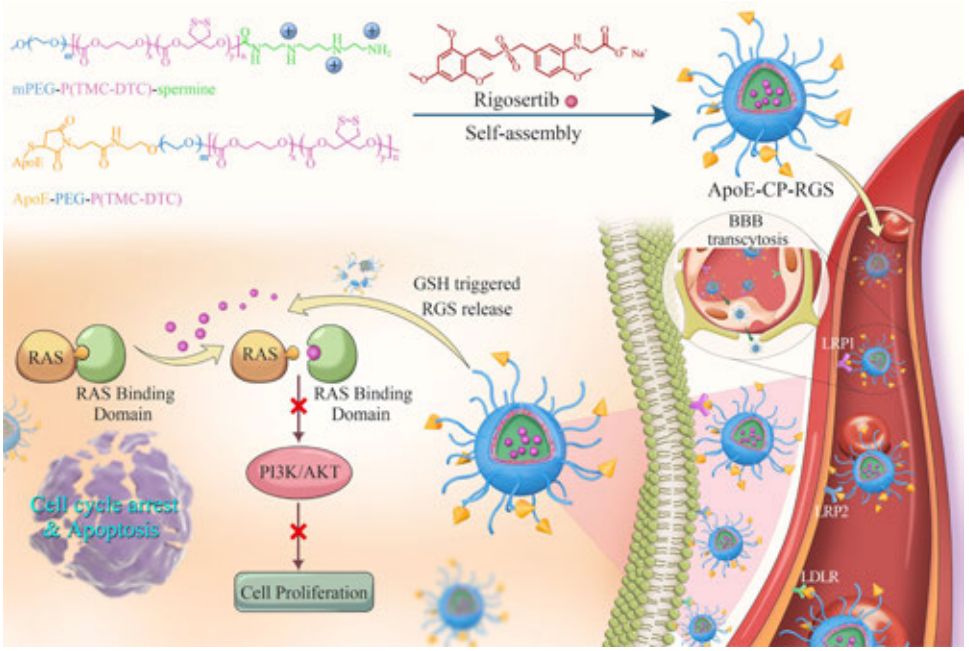

[a]ApoE-CP-RGS is made by self-assembly of poly(ethylene glycol)-*b*-poly(trimethylene carbonate-*co*-dithiolane trimethylene carbonate)−spermine (PEG−P(TMC-DTC)−spermine) and ApoE−PEG−P(TMC-DTC). ApoE ligand affords effective crossing of blood−brain barriers and GBM membrane via LDLRs (including LDLR, LRP-1, and LRP-2)-mediated transcytosis and endocytosis, respectively. GSH-triggered RGS release from ApoE-CP-RGS inside the GBM cells leads to an efficient inhibition of interactions of RAS and effector proteins, inducing cell cycle arrest and apoptosis.

We recently found that apolipoprotein E derived peptide (ApoE) mediated superior BBB crossing and targeted delivery of protein toxin to GBM compared with angiopep-2 peptide.[38] ApoE peptide has a high affinity to low-density lipoprotein receptors (LDLRs) family including LRP-1, LRP-2, and LDLR,[39] which are overexpressed on not only BBB but also GBM cells. Here, we report on RGS-loaded ApoE-targeted chimaeric polymersomes (ApoE-CP-RGS) for safe and highly potent treatment of human GBM in mice (Scheme 1). Notably, RGS is an amphipathic small molecule and can hardly be loaded into vehicles including micelles and polymersomes. Our results demonstrate that RGS can be efficiently loaded into ApoE-CP likely through charge interactions with cationic spermine in the watery core, similar to previous reports for methotrexate and pemetrexed.[40,41] More importantly, ApoE-CP-RGS displays remarkable anti-GBM efficacy both in vitro and in vivo. To the best of our knowledge, this is the first attempt to treat GBM with RAS inhibitors.

EXPERIMENTAL SECTION

Preparation and Characterization of ApoE-CP-RGS. RGS was readily loaded into the aqueous lumen of ApoE-CP via a solvent-exchange method. Briefly, 4.0 mg of PEG−P(TMC-DTC)−spermine and ApoE−PEG−P(TMC-DTC) at a molar ratio of 4:1 was dissolved in 100 μL of dimethylformamide and then slowly added into 900 μL of *N*-(2-hydroxyethyl)piperazine-*N*′-ethanesulfonic acid (HEPES, 5 mM, pH 6.8) containing 444 μg of RGS. The as-prepared mixture solution was further incubated overnight in a shaking bath (200 rpm, 37 °C, THZ-C, Taicang Instrument, China) to allow the formation of ApoE-CP-RGS via the self-assembly and self-cross-linking of the two copolymers. ApoE-CP-RGS was further purified through intensive dialysis against PB (10 mM, pH 7.4). Nontargeted CP-RGS was similarly acquired through solvent-exchange method from PEG−P(TMC-DTC)−spermine copolymer only.

The drug-loading content (DLC) and drug-loading efficiency (DLE) of polymersomes for RGS were measured by UV−vis absorption at 310 nm. A calibration curve was obtained by measuring the absorption of the RGS standard solutions with concentrations of 2−25 μg/mL. The DLC and DLE were determined according to the following formula

$$\text{DLC (wt \%)} = (\text{weight of loaded RGS/total weight of RGS and polymer}) \times 100$$

$$\text{DLE (\%)} = (\text{weight of loaded RGS/weight of RGS in feed}) \times 100$$

Considering that ApoE-CP-RGS following systemic administration would often encounter serum and high volume dilution in practical application, differential scanning calorimetry (DLS) was employed to monitor the size changes of ApoE-CP-RGS under the two conditions. Briefly, ApoE-CP-RGS (4.0 mg/mL) was dispersed in HEPES (5.0 mM, pH 6.8) containing 10% fetal bovine serum (FBS) and then settled down in a shaker (200 rpm, 37 °C) for 24 h. The size and size distribution were measured by DLS. Similarly, the size changes of ApoE-CP-RGS at different concentrations ranging from 1.0 to 0.01 mg/mL were monitored by DLS. To evaluate the reduction sensitivity, ApoE-CP-RGS was dispersed in a phosphate-buffered saline (PBS) solution containing 10 mM GSH. The samples were incubated in a shaker (200 rpm, 37 °C) for 4 h and then measured using DLS.

DOI: 10.1021/acs.molpharmaceut.9b00691
Mol. Pharmaceutics 2019, 16, 3711−3719

BBB Transcytosis of ApoE-CP-RGS in Vitro. To simulate the in vivo GBM targeting of ApoE-CP-RGS, a bEnd.3 cell monolayer was established as an in vitro BBB model to assess the BBB transcytosis capability of ApoE-CP-RGS. Briefly, bEnd.3 cells (2×10^5 cells/well in the upper chamber containing 300 μL of Dulbecco's modified Eagle's medium (DMEM) culture medium) were cultured in transwell inserts on 24-well plates for about 72 h. The complete confluency of bEnd.3 cells was observed under a microscope, and the monolayer integrity was assessed by measuring the trans-endothelial electrical resistance (TEER) using an epithelial volt-ohmmeter (Millicell ERS, Millipore, MA). The bEnd.3 cell monolayers with a TEER of over 200 Ω/cm^2 were employed for transport studies.

U-87 MG glioblastoma cells (1×10^5 cells/well in the lower chamber containing 800 μL of DMEM culture medium) were seeded in a 24-well transwell substrate for 24 h. Cy5-labeled ApoE-CP-RGS and CP-RGS (Cy5: 200 μg/mL) were added to the upper chamber containing free FBS DMEM. The incubation was performed under a shake bath (37 °C, 50 rpm) for 24 h. Then, the U-87 MG cells of the lower chamber were collected and analyzed by flow cytometry at the FL2-channel.

Cell Cycle Arrest, Apoptosis, and Cytotoxicity of ApoE-CP-RGS. The cell cycle arrest capabilities of RGS, CP-RGS, and ApoE-CP-RGS were assessed in the U-87 MG cells. Briefly, the cells (1×10^5 cell/well) were seeded in 6-well plates for 48 h. Then, free RGS, ApoE-CP-RGS, and CP-RGS were added at a RGS concentration of 0.5 μg/mL, and the cells were cultured for 4 h. After removing the medium, the cells were cultured in a fresh medium for additional 20 h. The cells were digested by trypsin, washed with PBS for three times, and centrifuged (800 rpm × 5 min). The collected U-87 MG cells were slowly added into 95% ethyl alcohol on ice and then stored in fridge at 4 °C for 24 h. After centrifugation, the cells were resuspended in propidium iodide (PI) staining solution containing RNase A under dark condition at 37 °C for 30 min. The cells at different phases of cell cycle were analyzed using flow cytometry (488 nm).

To evaluate the cell apoptosis induced by RGS, the U-87 MG cells (2×10^5 cells/well) were seeded in 6-well plates for 24 h. After incubating with different RGS formulations (RGS concentration: 1.0 μg/mL) for 4 h, the cells were cultured in a fresh medium for another 44 h. Then, the cells were collected by treating with 0.25% trypsin, centrifuging at 800 rpm for 5 min, and washing twice with cold PBS. The cells following resuspension in 300 μL of the binding buffer were treated with Annexin V-FITC (5 μL) and propidium iodide (PI, 5 μL) at room temperature for 15 min in the dark, and the apoptotic cells were analyzed using flow cytometry within 1 h.

The cytotoxicity of ApoE-CP-RGS was investigated by 3-(4,5-dimethylthiazol-2-yl)-2,5-diphenyltetrazolium bromide (MTT) assays. The U-87 MG cells (3000 cells/well) were cultured in a 96-well plate using DMEM medium for 24 h. Free RGS, ApoE-CP-RGS, and CP-RGS were added at various different RGS concentrations and incubated for 4 h. After removing the medium, the cells were incubated with fresh medium for another 68 h and then treated with a MTT solution at a final concentration of 0.5 mg/mL at 37 °C for 4 h. The above medium was replaced with dimethyl sulfoxide (150 μL/well), and the absorbance of formazan was acquired by a microplate reader at 492 nm. The cell viability was defined as the percentages of viable cells compared with the viability of the PBS group.

Western Blot Analysis. The level of p-AKT in the U-87 MG cells was determined by Western blot studies. The U-87 MG cells (2×10^5 cells/well) seeded in a 6-well plate were cultured for 24 h in DMEM. The RGS-loaded polymersomes or free RGS (RGS concentration: 1.0 μg/mL) was added. After 4 h of incubation, the cells were cultured in fresh DMEM for an additional 44 h and then lysed with 1.0 mL of RIPA buffer (Beyotime Biotechnology, Nantong, China) containing protease (100×, 10 μL) and phosphatase (100×, 10 μL) inhibitors. The protein concentration of different samples was detected through BCA Protein Assay kit. Equal amounts of total proteins (30−50 μg) from the samples following mixing with loading buffer were boiled for 5 min, detached on a 12% sodium dodecyl sulfate-polyacrylamide gel electrophoresis, and transferred to a poly(vinylidene fluoride) membrane. The obtained membranes were blocked with 5% bovine serum albumin for 1 h at room temperature, washed with Tris-buffered saline/0.1% Tween-20 (TBST), and incubated with secondary antibodies overnight. The expression of protein was detected by electrochemiluminescence assay (Millipore, Billerica, MA).

In Vivo Antitumor Experiments. The mice were handled under protocols approved by Soochow University Laboratory Animal Center and the Animal Care and Use Committee of Soochow University. In vivo antitumor efficacy was evaluated in orthotopic GBM xenografts that were established in two steps: (i) injection of the U-87 MG cells transformed with luciferase gene (U-87 MG-Luc) to the flank of BALB/c nude mice at the density of 2×10^6 cells/mouse to acquire tumor blocks in one month and (ii) injection of the U-87 MG-Luc tumor tissue fragments from the flank model using a 24# trocar into the left skull (2 mm lateral to the bregma and 3 mm depth) of deeply anesthetized (pentobarbital sodium, 40 mg/mL, 6−10 μL/g) mice. The day of implanting tumor tissue was designated as day 0. The mice bearing orthotopic glioblastoma tumor were divided into six groups (9 mice/group) and injected intravenously with different formulations (free RGS, CP-RGS, and ApoE-CP-RGS) via tail vein on day 8. The administration was once in 3 days for a total four doses. One mouse from each group was treated via the tail vein with Evans Blue staining (2%, 4 mL/kg), which was allowed to circulate for 30 min. Then, the mouse was sacrificed, and the main organs were excised and fixed in 4% formalin solution. Hematoxylin−eosin staining (H&E) and dUTP Nick-end labeling (TUNEL) were made by Servicebio Company (Shanghai, China), and the images were taken by Inverted fluorescence microscope (Leica QWin, Germany).

GBM-Targeting Ability Studies. The GBM-targeting ability studies were carried out by intravenous injection of Cy5-labeled CP, ApoE-CP, or ApoE-CP-RGS into orthotopic U-87 MG-Luc tumor-bearing female BALB/c mice (40 μg Cy5 equiv/animal). Three mice per group were employed to validate the results. The fluorescence images of mice were acquired at 24 h postinjection using an in vivo near-infrared fluorescence imaging system (Kodak, Rochester, New York) with λ_{Ex} = 747 nm and λ_{Em} = 774 nm.

For ex vivo imaging, glioblastoma-bearing mice were sacrificed immediately after in vivo imaging to acquire the brain tissue. The excised brains containing GBM were fixed in paraformaldehyde (4%, 24 h) and sliced into 5 μm thick tissue by Servicebio company (Shanghai, China). The cell nuclei were stained with 4′,6-diamidino-2-phenylindole (1 μg/mL) for 10 min. The distribution of Cy5-labeled CP, ApoE-CP, and

DOI: 10.1021/acs.molpharmaceut.9b00691
Mol. Pharmaceutics 2019, 16, 3711−3719

ApoE-CP-RGS in tumor area was observed using a confocal microscope (Leica TCS SP2).

Statistical Analysis. All data were presented as mean ± standard deviation. Statistical comparisons were performed by analysis of variance among the groups. Statistical significance was defined as $p < 0.05$, the survival data were performed by GraphPad Prism 7 using the Kaplan Meier method ($^{*}p < 0.05$, $^{**}p < 0.01$, $^{***}p < 0.01$).

RESULTS AND DISCUSSION

Fabrication of ApoE-CP-RGS and Triggered Drug Release. ApoE-CP-RGS was easily fabricated by solvent-exchange method from 20 mol % ApoE−PEG−P(TMC-DTC) (M_n = 5.0−(15.0−2.0) kg/mol) and 80 mol % PEG−P(TMC-DTC)−spermine (M_n = 5.0−(15.0−2.0)−0.2 kg/mol). We have previously shown that polymersomes containing 20 mol % ApoE−PEG−P(TMC-DTC) had the best targetability toward U-87 MG cells and optimal BBB permeability in vivo.[38] ApoE−PEG−P(TMC-DTC) copolymer was acquired by conjugating ApoE peptide (sequence: $(LRKLRKRLL)_2C$) to Mal−PEG−P(TMC-DTC) through Michael-type addition reaction. The functionality of ApoE peptide determined by bicinchoninic acid (BCA) assay was 98%. Of note, it is hard to find appropriate carriers for RGS due to its small and amphipathic nature. The amount of RGS loaded in polymersomes was determined by UV (310 nm). The results showed that the drug-loading efficiency (DLE) was about 57 and 52% for ApoE-CP-RGS and CP-RGS, respectively, at a theoretical drug-loading content of 10 wt % (Table S1). The decent RGS-loading level in ApoE-CP is mainly attributed to the strong ionic interactions and hydrogen bonding between spermine and RGS. ApoE-CP-RGS exhibited a small size (56−60 nm), low polydispersity, vesicular structure, and spherical morphology (Figure 1A). With disulfide cross-linking, ApoE-CP-RGS exhibited outstanding colloidal stability with negligible size changes against 100-fold dilution and 10% fetal bovine serum (FBS) (Figure 1B). In the presence of 10 mM GSH, ApoE-CP-RGS was enlarged in 4 h resulting from the cleavage of disulfide cross-links in the membrane of polymersomes (Figure 1C).

In vitro release experiments revealed that over 75% of RGS was released from both ApoE-CP-RGS and CP-RGS in the presence of 10 mM GSH within 24 h, although less than 21% of RGS was released in PBS without GSH under otherwise same conditions (Figure 1D). These results indicate that ApoE-CP-RGS could achieve a swift release of RGS under intracellular reduction environment, as a result of efficient cleavage of disulfide cross-links in vesicle membrane. The bioresponsive release of drugs and proteins has been reported for DTC-containing micelles[42,43] and polymersomes.[44−46]

BBB Transcytosis and Cellular Uptake of ApoE-CP-RGS in U-87 MG Cells. BBB transport as a critical factor for glioblastoma therapy was evaluated using an in vitro BBB model. To facilitate the observation, ApoE-CP-RGS and CP-RGS were labeled with cyanine 5 (Cy5) and denoted as ApoE-CP-RGS-Cy5 and CP-RGS-Cy5, respectively. Interestingly, ApoE-CP-RGS-Cy5 was observed to efficiently penetrate the in vitro BBB model formed by brain capillary endothelial cells and further target the U-87 MG cells. In comparison with CP-RGS-Cy5, ApoE-CP-RGS-Cy5 displayed a 5.3-fold higher cellular uptake in the U-87 MG cells within 24 h after passing through the BBB monolayer (Figure 2A). The remarkably boosted BBB penetration mainly resulted from the active targeting of ApoE-CP-RGS-Cy5 toward low-density lipoprotein receptor-related protein family (LDLRs) overexpressing on brain capillary endothelial cells. The excellent targetability of ApoE to LDLRs has been previously employed

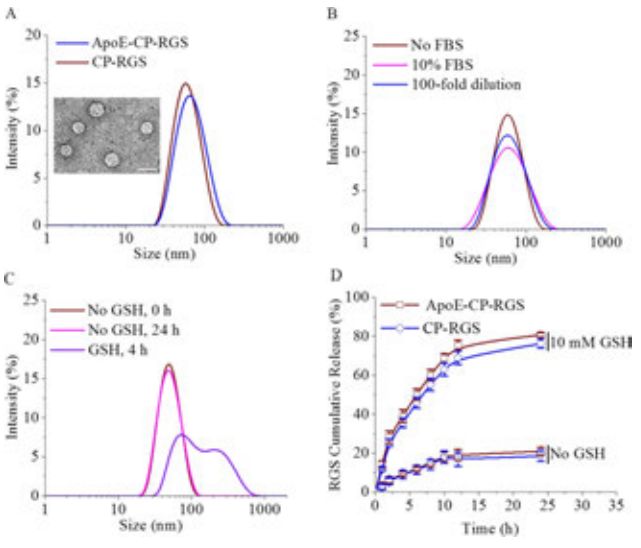

Figure 1. Physiochemical properties of ApoE-CP-RGS. (A) Size distribution of CP-RGS and ApoE-CP-RGS. Inset: Transmission electron microscopy image of ApoE-CP-RGS (bar: 100 nm). (B) Colloidal stability of ApoE-CP-RGS in serum and under 100-fold dilution. (C) Size changes of ApoE-CP-RGS induced by 10 mM GSH. (D) GSH-dependent release of RGS from ApoE-CP-RGS and CP-RGS.

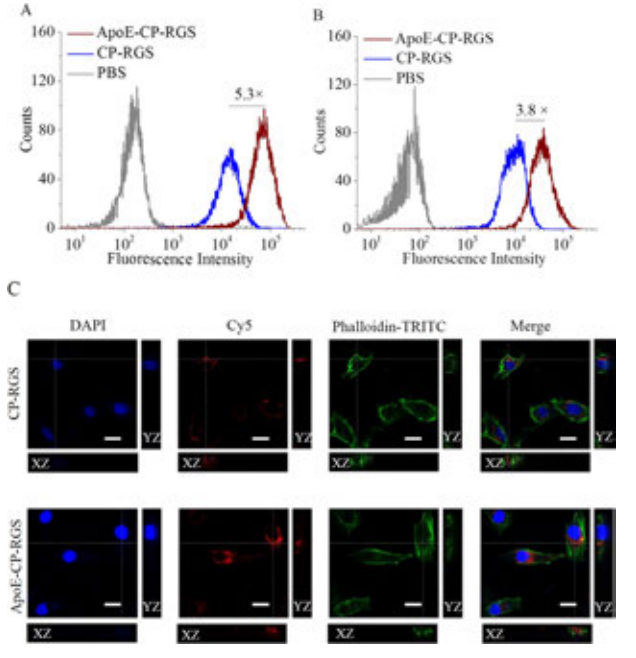

Figure 2. (A) Cellular uptake behaviors of CP-RGS-Cy5 and ApoE-CP-RGS-Cy5 in the U-87 MG within 24 h following the penetration of the in vitro BBB model (a bEnd.3 cell monolayer) measured by flow cytometry. (B) Cellular uptake of CP-RGS-Cy5 and ApoE-CP-RGS-Cy5 in the U-87 MG cells within 4 h measured by flow cytometry. (C) CLSM z-stack images of the U-87 MG cells after 4 h incubation with ApoE-CP-RGS-Cy5 and CP-RGS-Cy5. The cytoskeleton was stained with phalloidin-TRITC. Scale bar: 20 μm.

DOI: 10.1021/acs.molpharmaceut.9b00691
Mol. Pharmaceutics 2019, 16, 3711−3719

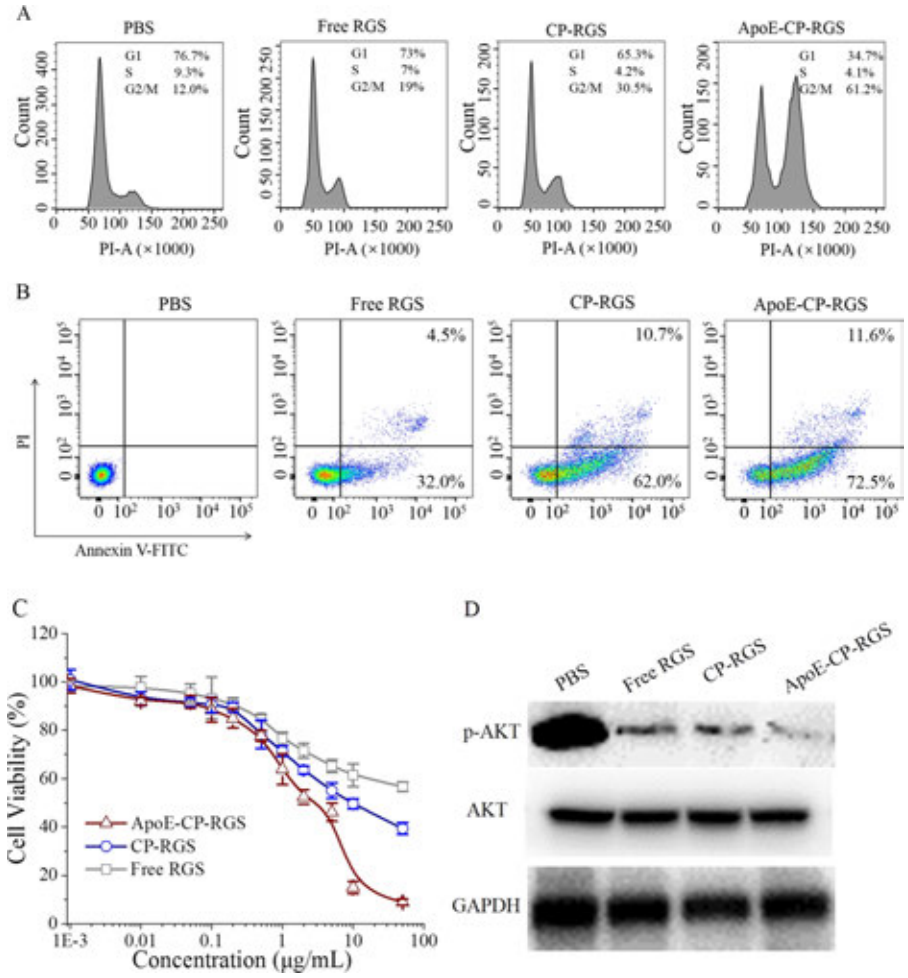

Figure 3. Cell cycle arrest (A), apoptosis (B), cytotoxicity (C), and Western blot analysis (D) of the U-87 MG cells treated with PBS, free RGS, CP-RGS, and ApoE-CP-RGS.

to facilitate the BBB transcytosis of several ApoE-decorated nanosystems.[39,47−49]

The cellular uptake profiles of polymersomes in the U-87 MG cells were examined by flow cytometry. Figure 2B shows that ApoE-CP-RGS-Cy5 had a 3.8-fold higher cellular uptake in the U-87 MG cells compared with that in CP-RGS-Cy5 following 4 h incubation, indicating that ApoE peptide facilitates the uptake of polymersomes. Confocal microscopy revealed that the U-87 MG cells following 4 h incubation with ApoE-CP-RGS generated a strong Cy5 fluorescence in the cytosol, while a weak Cy5 fluorescence was observed in cells treated with CP-RGS (Figure S1). The z-stack imaging of the cells following cytoskeleton staining with phalloidin-TRITC further demonstrated that Cy5 fluorescence of ApoE-CP-RGS was derived from the cytosol of the U-87 cancer cells, signifying significant cellular uptake and endosomal escape (Figure 2C). The superior endosomal escape of ApoE-CP-RGS can be attributed to the cationic and hydrophobic structure of ApoE ($(LRKLRKRLL)_2C$) that benefits the membrane fusion of polymersomes in the endosomal compartment. With similar structure, cationic lipid-based nanoparticles have been observed to possess high fusogenic activity, affording efficient cytosolic delivery of siRNA and mRNA in vivo.[50,51]

Cell Cycle Arrest, Apoptosis, and Cytotoxicity of ApoE-CP-RGS. RGS has been reported to induce G2/M phase arrest of cancer cells by inactivating PI3K-Akt pathway.[52−54] The cell cycle arrest effect of ApoE-CP-RGS was explored in the U-87 MG cells using flow cytometry. Figure 3A shows that free RGS, CP-RGS, and ApoE-CP-RGS induced obvious G2/M block at a RGS concentration of 0.5 μg/mL. In sharp contrast to slightly increased cells at the G2/M stage from 12 to 19% by free RGS in comparison with the PBS group, CP-RGS revealed noticeably increased cells at the G2/M stage up to 30.5%, which was further elevated to 61.2% by the introduction of ApoE peptide. The remarkable G2/M phase arrest of the U-87 cancer cells induced by ApoE-CP-RGS results from its efficient cellular uptake, which induces the inactivation of PI3K-Akt pathway and therefore apoptosis of cancer cells. We further evaluated the apoptosis of the U-87 MG cells induced by ApoE-CP-RGS following the PI and Annexin V double staining. The cells treated with ApoE-CP-RGS exhibited 72.5% of early apoptosis and 11.6% of late apoptosis (Figure 3B), which were much higher than those of the free RGS and CP-RGS groups, supporting an efficient cellular uptake of ApoE-CP-RGS and a swift release of RGS in the U-87 MG cells.

The in vitro anti-glioblastoma effect of ApoE-CP-RGS was investigated by MTT assays in the U-87 MG glioblastoma cells. Figure 3C demonstrates that ApoE-CP-RGS induced remarkable cytotoxicity with a half-maximal inhibitory concentration (IC_{50}) of 2.8 μg/mL, which was 3.5-fold lower

DOI: 10.1021/acs.molpharmaceut.9b00691
Mol. Pharmaceutics 2019, 16, 3711−3719

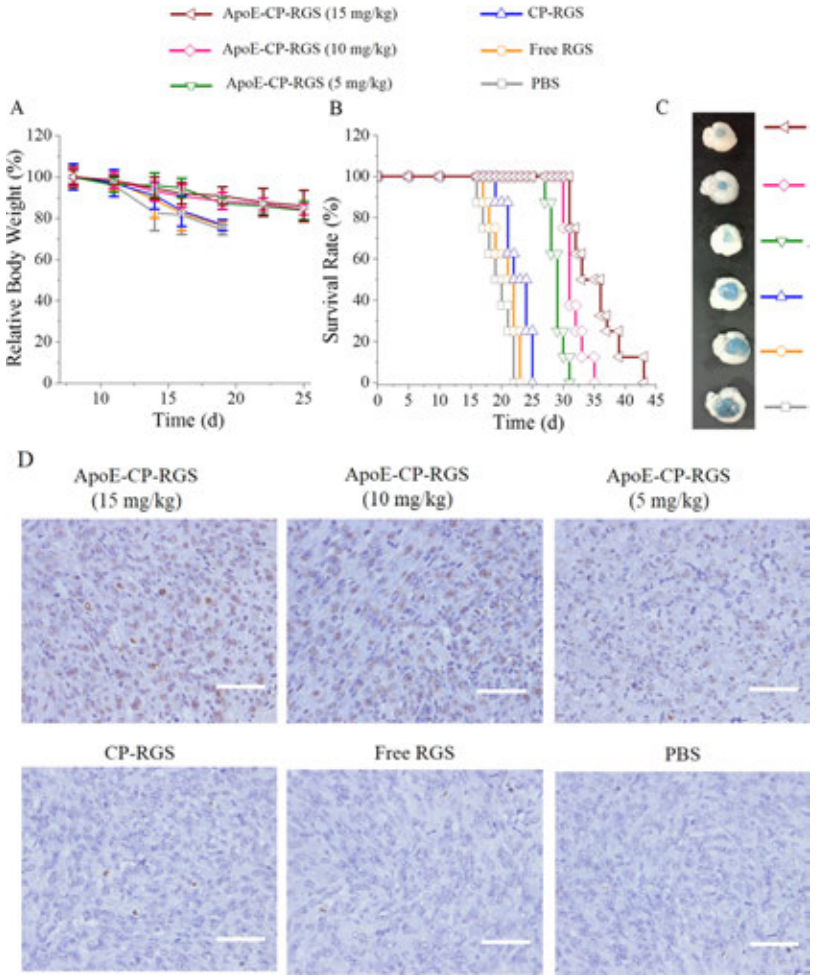

Figure 4. Antitumor efficacy of ApoE-CP-RGS in orthotopic glioblastoma xenografts. Different formulations were administrated on days 8, 11, 14, and 17. (A) Body weight changes of mice with time (n = 8). (B) Kaplan−Meier survival curve of the orthotopic glioblastoma-bearing mice analysis (log−rank test): ApoE-CP-RGS (5 mg/mg) vs CP-RGS ***p < 0.001 and ApoE-CP-RGS (15 mg/mg) and ApoE-CP-RGS (10 mg/mg) vs CP-RGS ****p < 0.0001. (C) Images of brains harvested from orthotopic glioblastoma-bearing nude mice on day 19 following Evans blue staining. (D) TUNEL assay of the brain tumor tissue sections harvested from orthotopic glioblastoma-bearing nude mice on day 19 (bar: 100 μm).

than that of CP-RGS. The enhanced cytotoxicity of ApoE-CP-RGS is mainly derived from ApoE, which boosted the cellular uptake of RGS-loaded nanosystems. Interestingly, cells treated with free RGS even at a maximum concentration of 50 μg/mL still exhibited a high cell viability (~60%) possibly owing to insufficient cellular uptake, signifying the importance of the ApoE-CP nanosystem for RGS delivery.

Level of Relative Proteins in Vitro. RGS, a PI3K/AKT pathway inhibitor, has been reported to be able to interfere with RAS-binding domains (RBD) and inhibit the p-AKT protein levels, causing a G2/M cell cycle arrest and apoptosis.[28] Here, we investigated the p-AKT protein levels of the U-87 MG glioblastoma cells treated with different formulations using Western blot analysis. Figure 3D demonstrates significantly downregulated levels of p-AKT protein in cells treated with free RGS, CP-RGS, and ApoE-CP-RGS at the RGS concentration of 1 μg/mL. Moreover, the levels of p-AKT in the cells follow the order ApoE-CP-RGS < CP-RGS < free RGS. The strongest inhibition of the p-AKT protein levels by ApoE-CP-RGS leads to its most apoptosis and highest cytotoxicity in the U-87 MG cells. Notably, PI3K-Akt signaling pathway has been reported to be closely associated with the pathogenesis of GBM,[55−57] and GBM patients with enhanced activation of PI3K-Akt signaling pathway generally display worse prognosis.[58,59] Thus, ApoE-CP-RGS with potent inhibition of the PI3K-Akt signaling pathway has great potential in GBM therapy.

Glioblastoma-Targeting Ability in Vivo. The in vivo accumulation of ApoE-CP in orthotopic GBM was monitored by near-infrared fluorescence imaging. Figure S2 displays the clear bioluminescence derived from the U-87 MG-Luc tumor cells in the brain of all mice, supporting the successful establishment of the orthotopic GBM. Notably, the mice administered with Cy5-labeled ApoE-CP and ApoE-CP-RGS demonstrated a strong Cy5 fluorescence at the GBM sites (Figure S2), signifying that ApoE confers the polymersomes with excellent GBM targetability and that RGS loading does not compromise their tumor targetability. In sharp contrast, the polymersomes without an ApoE decoration (CP) revealed little Cy5 fluorescence in the brain. Ex vivo imaging further confirmed that ApoE-CP and ApoE-CP-RGS induced a much higher accumulation at the GBM sites than did CP (Figure S2). Immunohistochemical assay showed that significant amounts of ApoE-CP and ApoE-CP-RGS infiltrated both the superfical and central areas of the GBM 24 h after injection, while CP revealed little accumulation and retention in the

DOI: 10.1021/acs.molpharmaceut.9b00691
Mol. Pharmaceutics 2019, 16, 3711−3719

tumor sites (Figure S3). These results have demonstrated that ApoE-CP with LDLR targetability facilitates the BBB transcytosis and active drug delivery toward GBM in vivo.

Anti-glioblastoma Effect in Vivo. The anti-glioblastoma effect of ApoE-CP-RGS was investigated using orthotopic glioblastoma xenografts in mice. Figure 4A displays that around 25% body weight loss was detected within 19 day for PBS, free RGS, and CP-RGS groups due to malignant glioblastoma invasion. In contrast, the mice treated with ApoE-CP-RGS had a much less body weight loss, corroborating the effective growth suppression of glioblastoma. Consistently, ApoE-CP-RGS displayed a prolonged survival time than PBS, free RGS, and CP-RGS groups (Figure 4B). Increasing the dosage of ApoE-CP-RGS induced an extended survival time, in which the mice treated with ApoE-CP-RGS at dosages of 5, 10, and 15 mg/kg had a medium survival time of 29, 31, and 34.5 day, respectively. On the contrary, the mice treated with PBS, free RGS, and CP-RGS revealed a medium survival time of 19.5, 21.5, and 23 day, respectively. Evans blue staining further showed that the mice treated with ApoE-CP-RGS had small tumor blocks in the brain, while PBS, free RGS, and CP-RGS all presented big tumor blocks (Figure 4C). The superior anti-glioblastoma efficacy of ApoE-CP-RGS is closely associated with their effective BBB penetration capacity and tumor targetability. The anti-glioblastoma effect was further verified by a significantly large area apoptosis in the tumor tissue of the mice treated with ApoE-CP-RGS using TUNEL assays (Figure 4D). H&E staining revealed that the mice treated with ApoE-CP-RGS had little damage on major organs (heart, liver, spleen, lung, kidney, etc.) (Figure S4). ApoE-CP-RGS consisting of ApoE that induces BBB transcytosis as well as selective targetability to glioblastoma, and oncoprotein inhibitor RGS that affords potent therapeutic efficacy as well as being nontoxic to healthy tissues holds great potential for safe and efficient treatment of glioblastoma.

CONCLUSIONS

We demonstrate that ApoE-functionalized chimaeric polymersomes (ApoE-CP) can efficiently encapsulate and transport oncoprotein inhibitor rigosertib into the orthotopically xenografted human GBM in mice, achieving high-efficacy and nontoxic GBM therapy. To the best of our knowledge, this is the first report on the application of rigosertib for treating GBM. Unlike previously reported cytotoxic drug nanoformulations, rigosertib-loaded ApoE-CP has a high selectivity and causes little side effects. Notably, ApoE-CP not only enhances the G2/M phase arrest and apoptosis of the U-87 MG cells with rigosertib but also greatly improves the BBB penetration and glioblastoma targetability of rigosertib in vivo, significantly prolonging the median survival time of mice. The combination of BBB-permeable chimaeric polymersomes and oncoprotein inhibitor appears to be a potential strategy for glioblastoma-targeted therapy.

ASSOCIATED CONTENT

Supporting Information

The Supporting Information is available free of charge on the ACS Publications website at DOI: 10.1021/acs.molpharmaceut.9b00691.

Materials, characterization, and experimental methods on cell culture and animal study, polymer synthesis, in vitro drug release, cellular uptake, and GBM-targeting ability; physicochemical properties of polymersomes with/without drug; images of CLSM; bioluminescence; in vivo fluorescence imaging; ex vivo fluorescence imaging; and immunohistochemical fluorescence assay (PDF)

AUTHOR INFORMATION

Corresponding Authors

*E-mail: cdeng@suda.edu.cn. Tel: +86-512-65884933 (C.D.).
*E-mail: zyzhong@suda.edu.cn. Tel: +86-512-65880098 (Z.Z.).

ORCID

Chao Deng: 0000-0001-7697-9874
Zhiyuan Zhong: 0000-0003-4175-4741

Notes

The authors declare no competing financial interest.

ACKNOWLEDGMENTS

This work was supported by the National Natural Science Foundation of China (NSFC 51773145, 51473110, 51633005, and 51761135117).

REFERENCES

(1) Stupp, R.; Hegi, M. E.; Gorlia, T.; et al. Cilengitide Combined with Standard Treatment for Patients with Newly Diagnosed Glioblastoma with Methylated MGMT Promoter (CENTRIC EORTC 26071-22072 Study): A Multicentre, Randomised, Open-Label, Phase 3 Trial. *Lancet Oncol.* **2014**, *15*, 1100−1108.

(2) Shergalis, A.; Bankhead, A., 3rd; Luesakul, U.; Muangsin, N.; Neamati, N. Current Challenges and Opportunities in Treating Glioblastoma. *Pharmacol. Rev.* **2018**, *70*, 412−445.

(3) Muldoon, L. L.; Alvarez, J. I.; Begley, D. J.; Boado, R. J.; Del Zoppo, G. J.; Doolittle, N. D.; Engelhardt, B.; Hallenbeck, J. M.; Lonser, R. R.; Ohlfest, J. R.; et al. Immunologic Privilege in the Central Nervous System and the Blood-Brain Barrier. *J. Cereb. Blood Flow Metab.* **2013**, *33*, 13−21.

(4) Abbott, N.; Ronnback, L.; Hansson, E. Astrocyte-Endothelial Interactions at the Blood-Brain Barrier. *Nat. Rev. Neurosci.* **2006**, *7*, 41−53.

(5) Pachter, J. S.; de Vries, H. E.; Fabry, Z. The Blood-Brain Barrier and Its Role in Immune Privilege in the Central Nervous System. *J. Neuropathol. Exp. Neurol.* **2003**, *62*, 593−604.

(6) Ulbrich, K.; Hekmatara, T.; Herbert, E.; Kreuter, J. Transferrin- and Transferrin-Receptor-Antibody-Modified Nanoparticles Enable Drug Delivery across the Blood-Brain Barrier (BBB). *Eur. J. Pharm. Biopharm.* **2009**, *71*, 251−256.

(7) Clark, A. J.; Davis, M. E. Increased Brain Uptake of Targeted Nanoparticles by Adding an Acid-Cleavable Linkage between Transferrin and the Nanoparticle Core. *Proc. Natl. Acad. Sci. U.S.A.* **2015**, *112*, 12486−12491.

(8) Kang, T.; Jiang, M.; Jiang, D.; Feng, X.; Yao, J.; Song, Q.; Chen, H.; Gao, X.; Chen, J. Enhancing Glioblastoma-Specific Penetration by Functionalization of Nanoparticles with an Iron-Mimic Peptide Targeting Transferrin/Transferrin Receptor Complex. *Mol. Pharmaceutics* **2015**, *12*, 2947−2961.

(9) Liu, D.-z.; Cheng, Y.; Cai, R.-q.; Wang, W.-w.; Cui, H.; Liu, M.; Zhang, B.-l.; Mei, Q.-b.; Zhou, S.-y. The Enhancement of siPLK1 Penetration across BBB and Its Anti Glioblastoma Activity in Vivo by Magnet and Transferrin Co-Modified Nanoparticle. *Nanomedicine* **2018**, *14*, 991−1003.

(10) Jhaveri, A.; Deshpande, P.; Pattni, B.; Torchilin, V. Transferrin-Targeted, Resveratrol-Loaded Liposomes for the Treatment of Glioblastoma. *J. Controlled Release* **2018**, *277*, 89−101.

(11) Bell, R. D.; Winkler, E. A.; Singh, I.; Sagare, A. P.; Deane, R.; Wu, Z.; Holtzman, D. M.; Betsholtz, C.; Armulik, A.; Sallstrom, J.;

DOI: 10.1021/acs.molpharmaceut.9b00691
Mol. Pharmaceutics 2019, 16, 3711−3719

Berk, B. C.; Zlokovic, B. V. Apolipoprotein E Controls Cerebrovascular Integrity Via Cyclophilin A. *Nature* **2012**, *485*, 512−6.
(12) Dal Magro, R.; Albertini, B.; Beretta, S.; Rigolio, R.; Donzelli, E.; Chiorazzi, A.; Ricci, M.; Blasi, P.; Sancini, G. Artificial Apolipoprotein Corona Enables Nanoparticle Brain Targeting. *Nanomedicine* **2018**, *14*, 429−438.
(13) Rajora, M. A.; Ding, L.; Valic, M.; Jiang, W.; Overchuk, M.; Chen, J.; Zheng, G. Tailored Theranostic Apolipoprotein E3 Porphyrin-Lipid Nanoparticles Target Glioblastoma. *Chem. Sci.* **2017**, *8*, 5371−5384.
(14) Winkler, E. A.; Nishida, Y.; Sagare, A. P.; Rege, S. V.; Bell, R. D.; Perlmutter, D.; Sengillo, J. D.; Hillman, S.; Kong, P.; Nelson, A. R.; Sullivan, J. S.; Zhao, Z.; Meiselman, H. J.; Wendy, R. B.; Soto, J.; Abel, E. D.; Makshanoff, J.; Zuniga, E.; De Vivo, D. C.; Zlokovic, B. V. Glut1 Reductions Exacerbate Alzheimer's Disease Vasculo-Neuronal Dysfunction and Degeneration. *Nat. Neurosci.* **2015**, *18*, 521−530.
(15) Anraku, Y.; Kuwahara, H.; Fukusato, Y.; Mizoguchi, A.; Ishii, T.; Nitta, K.; Matsumoto, Y.; Toh, K.; Miyata, K.; Uchida, S.; Nishina, K.; Osada, K.; Itaka, K.; Nishiyama, N.; Mizusawa, H.; Yamasoba, T.; Yokota, T.; Kataoka, K. Glycaemic Control Boosts Glucosylated Nanocarrier Crossing the BBB into the Brain. *Nat. Commun.* **2017**, *8*, No. 1001.
(16) Ren, J.; Shen, S.; Wang, D.; Xi, Z.; Guo, L.; Pang, Z.; Qian, Y.; Sun, X.; Jiang, X. The Targeted Delivery of Anticancer Drugs to Brain Glioma by PEGylated Oxidized Multi-Walled Carbon Nanotubes Modified with Angiopep-2. *Biomaterials* **2012**, *33*, 3324−3333.
(17) Ruan, S.; Yuan, M.; Zhang, L.; Hu, G.; Chen, J.; Cun, X.; Zhang, Q.; Yang, Y.; He, Q.; Gao, H. Tumor Microenvironment Sensitive Doxorubicin Delivery and Release to Glioma Using Angiopep-2 Decorated Gold Nanoparticles. *Biomaterials* **2015**, *37*, 425−435.
(18) Gao, S.; Tian, H.; Xing, Z.; Zhang, D.; Guo, Y.; Guo, Z.; Zhu, X.; Chen, X. A Non-Viral Suicide Gene Delivery System Traversing the Blood Brain Barrier for Non-Invasive Glioma Targeting Treatment. *J. Controlled Release* **2016**, *243*, 357−369.
(19) Qiao, C.; Yang, J.; Shen, Q.; Liu, R.; Li, Y.; Shi, Y.; Chen, J.; Shen, Y.; Xiao, Z.; Weng, J.; Zhang, X. Traceable Nanoparticles with Dual Targeting and ROS Response for RNAi-Based Immunochemotherapy of Intracranial Glioblastoma Treatment. *Adv. Mater.* **2018**, *30*, No. 1705054.
(20) Israel, L. L.; Braubach, O.; Galstyan, A.; Chiechi, A.; Shatalova, E. S.; Grodzinski, Z.; Ding, H.; Black, K. L.; Ljubimova, J. Y.; Holler, E. A Combination of Tri-Leucine and Angiopep-2 Drives a Polyanionic Polymalic Acid Nanodrug Platform across the Blood-Brain Barrier. *ACS Nano* **2019**, *13*, 1253−1271.
(21) Tao, J.; Fei, W.; Tang, H.; Li, C.; Mu, C.; Zheng, H.; Li, F.; Zhu, Z. Angiopep-2-Conjugated "Core-Shell" Hybrid Nanovehicles for Targeted and pH-Triggered Delivery of Arsenic Trioxide into Glioma. *Mol. Pharmaceutics* **2019**, *16*, 786−797.
(22) Kurzrock, R.; Gabrail, N.; Chandhasin, C.; Moulder, S.; Smith, C.; Brenner, A.; Sankhala, K.; Mita, A.; Elian, K.; Bouchard, D.; Sarantopoulos, J. Safety, Pharmacokinetics, and Activity of GRN1005, a Novel Conjugate of Angiopep-2, a Peptide Facilitating Brain Penetration, and Paclitaxel, in Patients with Advanced Solid Tumors. *Mol. Cancer Ther.* **2012**, *11*, 308−316.
(23) Barbacid, M. RAS Genes. *Annu. Rev. Biochem.* **1986**, *56*, 779−827.
(24) Samatar, A. A.; Poulikakos, P. I. Targeting RAS−ERK Signalling in Cancer: Promises and Challenges. *Nat. Rev. Drug Discovery* **2014**, *13*, 928−942.
(25) Stephen, A. G.; Esposito, D.; Bagni, R. K.; McCormick, F. Dragging RAS Back in the Ring. *Cancer Cells* **2014**, *25*, 272−281.
(26) Van Cutsem, E.; Lenz, H. J.; Kohne, C. H.; Heinemann, V. Fluorouracil, Leucovorin, and Irinotecan Plus Cetuximab Treatment and RAS Mutations in Colorectal Cancer. *J. Clin. Oncol.* **2015**, *33*, 692−700.
(27) Jost, M.; Chen, Y.; Gilbert, L. A.; Horlbeck, M. A.; et al. Combined CRISPRi/a-Based Chemical Genetic Screens Reveal That Rigosertib Is a Microtubule-Destabilizing Agent. *Mol. Cell* **2017**, *68*, 210−223.
(28) Dietrich, P.; et al. Combined Effects of PLK1 and RAS in Hepatocellular Carcinoma Reveal Rigosertib as Promising Novel Therapeutic "Dual-Hit" Option. *Oncotarget* **2018**, *9*, 3605−3618.
(29) Chapman, C. M.; Sun, X.; Roschewski, M.; Aue, G.; et al. ON 01910.Na Is Selectively Cytotoxic for Chronic Lymphocytic Leukemia Cells through a Dual Mechanism of Action Involving PI3K/AKT Inhibition and Induction of Oxidative Stress. *Clin. Cancer Res.* **2012**, *18*, 1979−1991.
(30) Gumireddy, K.; Reddy, M. V.; Cosenza, S. C.; Boominathan, R.; Baker, S. J.; Papathi, N.; Jiang, J.; Holland, J.; Reddy, E. P. ON01910, a Non-ATP-Competitive Small Molecule Inhibitor of PLK1, Is a Potent Anticancer Agent. *Cancer Cells* **2005**, *7*, 275−286.
(31) Roschewski, M.; Farooqui, M.; Aue, G.; Wilhelm, F.; Wiestner, A. Phase I Study of ON 01910.Na (Rigosertib), a Multikinase PI3K Inhibitor in Relapsed/Refractory B-Cell Malignancies. *Leukemia* **2013**, *27*, 1920−1923.
(32) Athuluri-Divakar, S. K.; Vasquez-Del Carpio, R.; Dutta, K.; Baker, S. J.; Cosenza, S. C.; Basu, I.; Gupta, Y. K.; Reddy, M. V. R.; Ueno, L.; Hart, J. R.; Vogt, P. K.; Mulholland, D.; Guha, C.; Aggarwal, A. K.; Reddy, E. P. A Small Molecule RAS-Mimetic Disrupts RAS Association with Effector Proteins to Block Signaling. *Cell* **2016**, *165*, 643−655.
(33) Montalban-Bravo, G.; Garcia-Manero, G.; Jabbour, E. Therapeutic Choices after Hypomethylating Agent Resistance for Myelodysplastic Syndromes. *Curr. Opin. Hematol.* **2018**, *25*, 146−153.
(34) Anderson, R. T.; Keysar, S. B.; Bowles, D. W.; Glogowska, M. J.; et al. The Dual Pathway Inhibitor Rigosertib Is Effective in Direct Patient Tumor Xenografts of Head and Neck Squamous Cell Carcinomas. *Mol. Cancer Ther.* **2013**, *12*, 1994−2005.
(35) Montalbanbravo, G.; Garciamanero, G. Novel Drugs for Older Patients with Acute Myeloid Leukemia. *Leukemia* **2015**, *29*, 760−769.
(36) Ma, W. W.; Messersmith, W. A.; Dy, G. K.; Weekes, C. D.; Whitworth, A.; Ren, C.; Maniar, M.; Wilhelm, F.; Eckhardt, S. G.; Adjei, A. A.; Jimeno, A. Phase I Study of Rigosertib, an Inhibitor of the Phosphatidylinositol 3-Kinase and Polo-Like Kinase 1 Pathways, Combined with Gemcitabine in Patients with Solid Tumors and Pancreatic Cancer. *Clin. Cancer Res.* **2012**, *18*, 2048−2055.
(37) Dang, C. V.; Reddy, E. P.; Shokat, K. M.; Soucek, L. Drugging the 'Undruggable' Cancer Targets. *Nat. Rev. Cancer* **2017**, *17*, 502−508.
(38) Jiang, Y.; Zhang, J.; Meng, F.; Zhong, Z. Apolipoprotein E Peptide-Directed Chimeric Polymersomes Mediate an Ultrahigh-Efficiency Targeted Protein Therapy for Glioblastoma. *ACS Nano* **2018**, *12*, 11070−11079.
(39) Oller-Salvia, B.; Sanchez-Navarro, M.; Giralt, E.; Teixido, M. Blood-Brain Barrier Shuttle Peptides: An Emerging Paradigm for Brain Delivery. *Chem. Soc. Rev.* **2016**, *45*, 4690−4707.
(40) Yang, W.; Zou, Y.; Meng, F.; Zhang, J.; Cheng, R.; Deng, C.; Zhong, Z. Efficient and Targeted Suppression of Human Lung Tumor Xenografts in Mice with Methotrexate Sodium Encapsulated in All-Function-in-One Chimeric Polymersomes. *Adv. Mater.* **2016**, *28*, 8234−8239.
(41) Yang, W.; Yang, L.; Xia, Y.; Cheng, L.; Zhang, J.; Meng, F.; Yuan, J.; Zhong, Z. Lung Cancer Specific and Reduction-Responsive Chimaeric Polymersomes for Highly Efficient Loading of Pemetrexed and Targeted Suppression of Lung Tumor in Vivo. *Acta Biomater.* **2018**, *70*, 177−185.
(42) Zou, Y.; Fang, Y.; Meng, H.; Meng, F.; Deng, C.; Zhang, J.; Zhong, Z. Self-Crosslinkable and Intracellularly Decrosslinkable Biodegradable Micellar Nanoparticles: A Robust, Simple and Multifunctional Nanoplatform for High-Efficiency Targeted Cancer Chemotherapy. *J. Controlled Release* **2016**, *244*, 326−335.
(43) Zhu, Y.; Zhang, J.; Meng, F.; Cheng, L.; Feijen, J.; Zhong, Z. Reduction-Responsive Core-Crosslinked Hyaluronic Acid-b-Poly-(Trimethylene Carbonate-co-Dithiolane Trimethylene Carbonate) Micelles: Synthesis and CD44-Mediated Potent Delivery of Docetaxel

DOI: 10.1021/acs.molpharmaceut.9b00691
Mol. Pharmaceutics 2019, 16, 3711−3719

to Triple Negative Breast Tumor in Vivo. *J. Mater. Chem. B* **2018**, *6*, 3040−3047.
(44) Zou, Y.; Meng, F.; Deng, C.; Zhong, Z. Robust, Tumor-Homing and Redox-Sensitive Polymersomal Doxorubicin: A Superior Alternative to Doxil and Caelyx? *J. Controlled Release* **2016**, *239*, 149−158.
(45) Jiang, Y.; Yang, W.; Zhang, J.; Meng, F.; Zhong, Z. Protein Toxin Chaperoned by LRP-1-Targeted Virus-Mimicking Vesicles Induces High-Efficiency Glioblastoma Therapy in Vivo. *Adv. Mater.* **2018**, *30*, No. e1800316.
(46) Zhang, N.; Xia, Y.; Zou, Y.; Yang, W.; Zhang, J.; Zhong, Z.; Meng, F. ATN-161 Peptide Functionalized Reversibly Cross-Linked Polymersomes Mediate Targeted Doxorubicin Delivery into Melanoma-Bearing C57bl/6 Mice. *Mol. Pharmaceutics* **2017**, *14*, 2538−2547.
(47) Re, F.; Cambianica, I.; Zona, C.; Sesana, S.; et al. Functionalization of Liposomes with ApoE-Derived Peptides at Different Density Affects Cellular Uptake and Drug Transport across a Blood-Brain Barrier Model. *Nanomedicine* **2011**, *7*, 551−559.
(48) Wang, D.; El-Amouri, S. S.; Dai, M.; Kuan, C. Y.; Hui, D. Y.; Brady, R. O.; Pan, D. Engineering a Lysosomal Enzyme with a Derivative of Receptor-Binding Domain of ApoE Enables Delivery across the Blood-Brain Barrier. *Proc. Natl. Acad. Sci. U.S.A.* **2013**, *110*, 2999−3004.
(49) Boyé, K.; Pujol, N.; Alves, I. D.; Chen, Y. P.; Daubon, T.; Lee, Y. Z.; Dedieu, S.; Constantin, M.; Bello, L.; Rossi, M. The Role of CXCR3/LRP1 Cross-Talk in the Invasion of Primary Brain Tumors. *Nat. Commun.* **2017**, *8*, No. 1571.
(50) Sato, Y.; Hashiba, K.; Sasaki, K.; Maeki, M.; Tokeshi, M.; Harashima, H. Understanding Structure-Activity Relationships of pH-Sensitive Cationic Lipids Facilitates the Rational Identification of Promising Lipid Nanoparticles for Delivering siRNAs in Vivo. *J. Controlled Release* **2019**, *295*, 140−152.
(51) Sabnis, S.; Kumarasinghe, E. S.; Salerno, T.; Mihai, C.; Ketova, T.; Senn, J. J.; Lynn, A.; Bulychev, A.; McFadyen, I.; Chan, J.; Almarsson, O.; Stanton, M. G.; Benenato, K. E. A Novel Amino Lipid Series for mRNA Delivery: Improved Endosomal Escape and Sustained Pharmacology and Safety in Non-Human Primates. *Mol. Ther.* **2018**, *26*, 1509−1519.
(52) Liu, Z.; Li, H.; He, L.; Xiang, Y.; Tian, C.; Li, C.; Tan, P.; Jing, J.; Tian, Y.; Du, L.; Huang, Y.; Han, L.; Li, M.; Zhou, Y. Discovery of Small-Molecule Inhibitors of the HSP90-Calcineurin-NFAT Pathway against Glioblastoma. *Cell Chem. Biol.* **2019**, *26*, 352−365.
(53) Sánchez-Hernández, L.; Hernándezsoto, J.; Vergara, P.; González, R. O.; Segovia, J. Additive Effects of theCombined Expression of Soluble Forms of GAS1 and PTEN Inhibiting Glioblastoma Growth. *Gene Ther.* **2018**, *25*, 439−449.
(54) Zhang, G.; Li, D.; Chen, H.; Zhang, J.; Jin, X. Vitexin Induces G2/M phase Arrest and Apoptosis Via Akt/mTOR Signaling Pathway in Human Glioblastoma Cells. *Mol. Med. Rep.* **2018**, *17*, 4599−4604.
(55) Chakravarti, A.; Zhai, G.; Suzuki, Y.; Sarkesh, S.; Black, P. M.; Muzikansky, A.; Loeffler, J. S. The Prognostic Significance of Phosphatidylinositol 3-Kinase Pathway Activation in Human Gliomas. *J. Clin. Oncol.* **2004**, *22*, 1926−1933.
(56) Maira, S. M.; Stauffer, F.; Brueggen, J.; Furet, P.; et al. Identification and Characterization of NVP-BEZ235, a New Orally Available Dual Phosphatidylinositol 3-Kinase/Mammalian Target of Rapamycin Inhibitor with Potent in Vivo Antitumor Activity. *Mol. Cancer Ther.* **2008**, *7*, 1851−1863.
(57) Lefranc, F.; Brotchi, J.; Kiss, R. Possible Future Issues in the Treatment of Glioblastomas: Special Emphasis on Cell Migration and the Resistance of Migrating Glioblastoma Cells to Apoptosis. *J. Clin. Oncol.* **2005**, *23*, 2411−2422.
(58) Paw, I.; Carpenter, R. C.; Watabe, K.; Debinski, W.; Lo, H. W. Mechanisms Regulating Glioma Invasion. *Cancer Lett.* **2015**, *362*, 1−7.
(59) Li, X.; Wu, C.; Chen, N.; Gu, H.; et al. PI3K/Akt/mTOR Signaling Pathway and Targeted Therapy for Glioblastoma. *Oncotarget* **2016**, *7*, 33440−33450.

DOI: 10.1021/acs.molpharmaceut.9b00691
Mol. Pharmaceutics 2019, 16, 3711−3719